Naval Research Laboratory

Washington, DC 20375-5320

NRL/MR/5650--10-9243

A Study of Photoreceivers for Free-Space, Analog, Intensity-Modulated, Direct-Detection Optical Links Operating at Microwave Frequencies

FRANK BUCHOLTZ
WILL RABINOVICH

Photonics Technology Branch
Optical Sciences Division

CHARMAINE GILBREATH

Freespace Photonics Communications Office
Information Technology Division

September 10, 2010

REPORT DOCUMENTATION PAGE

Form Approved
OMB No. 0704-0188

1. REPORT DATE *(DD-MM-YYYY)*	**2. REPORT TYPE**	**3. DATES COVERED** *(From - To)*
10-09-2010	Memorandum Report	1 June 2009 - 31 October 2009

4. TITLE AND SUBTITLE

A Study of Photoreceivers for Free-Space, Analog, Intensity-Modulated, Direct-Detection Optical Links Operating at Microwave Frequencies

5a. CONTRACT NUMBER

5b. GRANT NUMBER

5c. PROGRAM ELEMENT NUMBER

6. AUTHOR(S)

F. Bucholtz, W. Rabinovich, and C. Gilbreath

5d. PROJECT NUMBER
062271N

5e. TASK NUMBER

5f. WORK UNIT NUMBER
56-6388-0-9

7. PERFORMING ORGANIZATION NAME(S) AND ADDRESS(ES)

Naval Research Laboratory
4555 Overlook Avenue, SW
Washington, DC 20375

*SFA, Inc.
2200 Defense Highway
Crofton, MD 21114

8. PERFORMING ORGANIZATION REPORT NUMBER

NRL/MR/5650--10-9243

9. SPONSORING / MONITORING AGENCY NAME(S) AND ADDRESS(ES)

Office of Naval Research
One Liberty Center
875 North Randolph Street
Arlington, VA 22203-1995

10. SPONSOR / MONITOR'S ACRONYM(S)

ONR

11. SPONSOR / MONITOR'S REPORT NUMBER(S)

12. DISTRIBUTION / AVAILABILITY STATEMENT

Approved for public release; distribution is unlimited.

13. SUPPLEMENTARY NOTES

*SFA, Inc., 2200 Defense Highway, Crofton, MD 21114

14. ABSTRACT

We compared the RF performance of various photodetection architectures for free-space optical links in order to optimize link performance at microwave frequencies. The three architectures studied were a) a p-i-n photodiode with internal resistor, b) a p-i-n photodiode with internal resistor followed by a high-gain RF amplifier, and c) a p-i-n photodiode followed by a transimpedance amplifier (TIA). We also consider the use of an avalanche photodiode followed by either a TIA or an RF amplifier. We conclude that, in almost all cases, a p-i-n photodiode followed by a high-performance RF amplifier offers optimum performance.

15. SUBJECT TERMS

Optical fiber
Numerical aperture
Beam divergence

16. SECURITY CLASSIFICATION OF:			**17. LIMITATION OF ABSTRACT**	**18. NUMBER OF PAGES**	**19a. NAME OF RESPONSIBLE PERSON**
a. REPORT	**b. ABSTRACT**	**c. THIS PAGE**			Frank Bucholtz
Unclassified	Unclassified	Unclassified	UL	39	**19b. TELEPHONE NUMBER** *(include area code)* (202) 767-9342

Standard Form 298 (Rev. 8-98)
Prescribed by ANSI Std. Z39.18

Contents

Executive Summary

The purpose of this report is to compare the radio-frequency (RF) performance of various photodetection architectures for use in free-space analog photonic links. The motivation for this work was to understand how to optimize overall link performance at microwave frequencies. However, the results we obtain are applicable to any photonic link, including links employing optical fibers.

We first present the basic theory for an RF link employing a photonic segment. We then present experimental results comparing three photoreceiver architectures: 1) a p-i-n photodiode with internal load resistor; 2) a p-i-n photodiode with internal load resistor followed by a high-gain, RF electrical amplifier; and 3) a p-i-n photodiode followed by a transimpedance amplifier.

Finally, we perform calculations to predict the performance of a photoreceiver comprising an avalanche photodiode (APD) followed by an RF gain element (either a TIA or an RF amplifier. Typically, an APD is employed to provide gain internal to the photodiode and thus relieve the performance requirements for any external amplifier.

By comparing the RF link metrics of gain, noise figure, and linearity for these various architectures, we can assess the utility of any particular approach in any given link. **We conclude that an architecture comprising a p-i-n diode, with or without an internal load resistor, followed by a high-quality, high-gain RF amplifier is almost always the preferred receiver architecture.**

The discussion and experiments are limited to intensity-modulated, direct-detection photonic links.

1. Introduction

In this report we consider the issue of the optimum photoreceiver for use in an analog, radio-frequency (RF), free-space optical (FSO) link operating at frequencies at or above 1 GHz and employing intensity-modulation and direct detection (IMDD). Due to atmospheric turbulence, the received optical power can fluctuate by orders of magnitude and, for long-distance links, the maximum received optical power is often significantly less than 100 uW [Burr09, Buch09]. For digital FSO links operating at rates of a few hundred MBits/sec, a common photoreceiver is a p-i-n or avalanche photodiode with a built-in transimpedance amplifier (TIA) and often incorporating automatic gain control (AGC). Depending on the modulation format, AGC may or may not be permitted in an analog link and, in any case, AGC will produce turbulence-dependent distortion in the analog signal. By comparison, for fiber-optic based analog photonic links, the typical photoreceiver comprises a p-i-n photodiode followed by an RF amplifier.

Proper choice of photoreceiver for a FSO analog link can be quantified based on the overall RF gain, noise figure and linearity of the entire link. In this report we present the results of laboratory measurements on a fiber-optic analog photonic link using three different photoreceivers: 1) a reverse-biased p-i-n photodiode with internal load resistor; 2) a reverse-biased p-i-n photodiode with internal load resistor followed by an external, high-gain RF amplifier; and 3) a reverse-biased p-i-n photodiode with no internal load resistor but with a TIA built into the package.

We first summarize the theory for RF gain, noise figure and linearity in the general case of an analog photonic link and then apply the theory to links employing the photoreceivers studied here. We also present calculations for a photoreceiver comprising an avalanche photodiode (APD) followed by a gain element, either a TIA or an RF amplifier.

SI units are used throughout.

Manuscript approved November 20, 2009.

2. Theory

2.1 Review of RF Photonic Link Basics

Figure 1 shows a generic photonic link employing intensity modulation and direct detection. The intensity modulator transforms RF signals into intensity modulation of the optical beam and the photoreceiver transforms the intensity-modulated optical signal

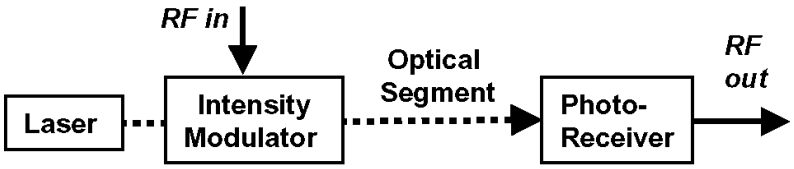

Fig. 1. Block diagram of a generic analog RF photonic link.

back into electrical RF signals. The optical segment of the overall link could be either free-space or optical fiber or, for that matter, any optical transmission medium. To facilitate comparison of various photodetection architecture later in this report, we will assume that what will be referred to as the "photonic link" will always contain a p-i-n diode as the means of photodetection. The photodiode produces photocurrent I proportional to received optical power. I comprises a DC photocurrent I_{DC} proportional to the time-averaged received optical power and an RF photocurrent i proportional to the product of I_{DC} and the RF modulation. For calculating RF link quantities, the critical system parameter is, in fact, the DC photocurrent I_{DC} [Buch08]. The modulator is characterized by a quantity V_π that represents the inverse efficiency in transforming electrical RF voltage into optical modulation. Lower V_π values indicate higher efficiency.

Expressions for the RF link parameters, written in terms of the electrical and optical parameters of the system, are summarized in Appendix 1. (Note: For all the

equations in Appendix 1, it is assumed that the intensity modulator is biased exactly at optical quadrature.) We have assumed that the optical modulation depth and received optical power are sufficiently small so that both the intensity modulator and the photodiode are operating linearly. Photodiode current *I(A)* resulting from received optical power $p_{opt}(W)$ is given by

$$I = \Re p_{opt} \tag{1}$$

where $\Re(A/W)$ is the RF-frequency-dependent responsivity. The (dimensionless) RF power gain of the photonic link is

$$G_{PL} = \left(\frac{g}{2^{2r}} \right) I_{DC}^2 \tag{2}$$

where $g = Z_i Z_o \left(\pi / V_\pi\right)^2$, Z_i and Z_o are the RF link input and output impedances, respectively, and where the factor *r* depends on the details of the photodetector circuit as discussed in detail below.

The (dimensionless) RF noise factor (or noise figure) is

$$NF = \frac{PSD_{noise}}{G_{PL} kT} \tag{3}$$

where $PSD_{noise}\left(W / Hz\right)$ is the electrical power spectral density of noise, from all sources, observed at the photodetector output, *k* is Boltzmann's constant (*1.38 e –23 J/K*), and *T* is the receiver temperature (K).

The third-order output intercept point $OIP3(W)$ resulting from third-order intermodulation, is given by

$$OIP3 = \left(4/2^{2r}\right) I_{DC}^2 Z_o \tag{4}$$

Finally, the intermodulation third-order spurious-free dynamic range $SFDR3\left(Hz^{2/3}\right)$ is

$$SFDR3 = \left(\frac{OIP3}{PSD_{noise}}\right)^{2/3}. \tag{5}$$

In order to obtain expressions for the r-parameter we consider the two specific photodetector RF circuits shown in Fig 2. In Fig 2a, the RF photocurrent passes directly to the external load (e.g. an electrical spectrum analyzer), while in Fig 2b, the RF photocurrent is divided between the internal load Z_{int} and the external load. The internal load helps to flatten the frequency response of the diode and its value is usually near 50 ohms so that, when the detector is attached to a 50 ohm external load, the RF photocurrent is equally divided between internal and external loads. For these two cases we have a) No internal load: $r = 0$, and b) internal 50 ohm load: $r = 1$.

Once V_π, Z_i and Z_o are known for a particular photonic link, Eqs 1, 2 and 4 allow the RF gain and OIP3 to be determined for any received optical power level, that is, for any I_{DC}. Figure 3a and 3b show the calculated RF gain and OIP3, respectively, for an IM-DD photonic link as a function of I_{DC} for $1nA \le I_{DC} \le 1mA$ for various combinations of V_π and *r*. For most RF applications, the gain and *OIP3* values shown in Fig. 3 are exceedingly poor thus demonstrating that the utilization of a photonic link for transmission of analog information presents significant challenges. By making simplifying assumptions about the noise, the noise figure can also be calculated as a function of I_{DC}. This will be addressed in the next section.

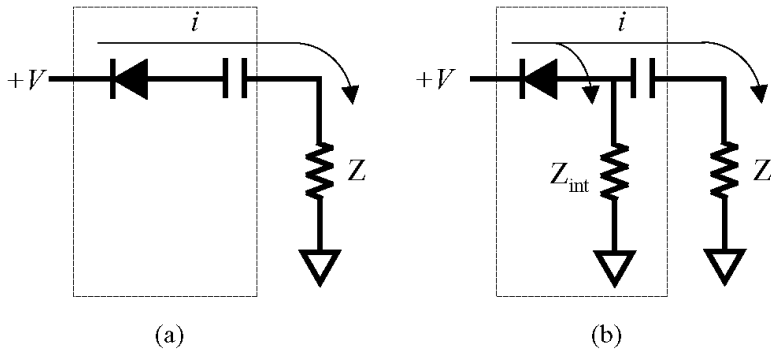

Fig. 2. Two common photodiode / electrical load configurations. (a) No internal load resistor. RF photocurrent i flows directly flows directly to external load Z. (b) With internal load resistor RF photocurrent is split between internal and external loads.

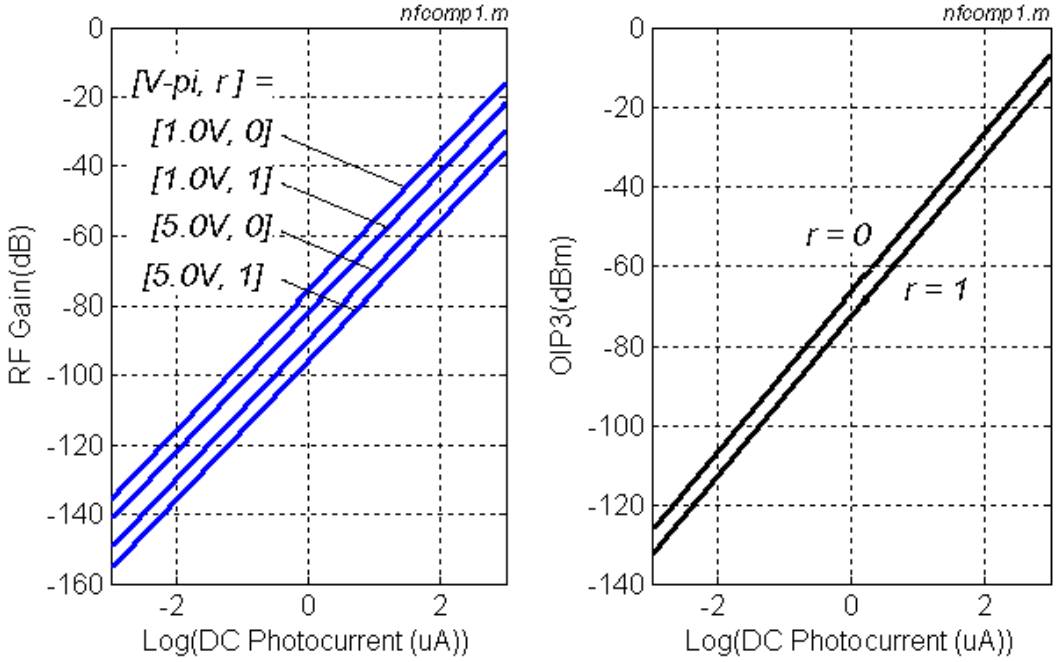

Fig. 3. (a) RF gain as function of DC photocurrent for various combinations of V_π and r-parameter (see text) (b) Third-order output intercept power as a function of DC photocurrent for various values of the r-parameter.

2.2 Cascade Parameter Analysis

Consider now a series cascade of RF gain elements as shown in Fig. 3a, with the i-th element characterized by parameters G_i, NF_i, and $OIP3_i$. We seek the overall values of G, NF, and $OIP3$. This is the well-known problem of cascaded RF amplifiers and the results are immediately applicable here [Uric09]. The cascaded gain is simply the product

$$G_{total} = G_1 G_2 \cdots G_N \,, \tag{6a}$$

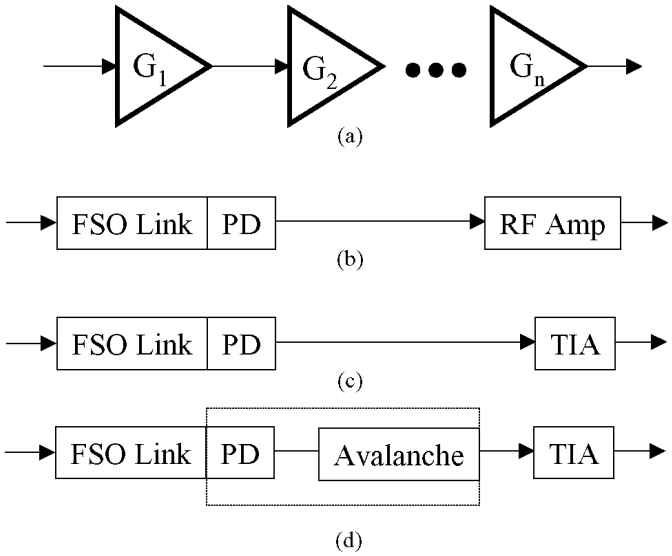

Fig. 4. (a) Generic representation of a cascaded chain of gain element; (b) cascaded chain of gain elements in an analog photonic link (including p-i-n photodiode) and external RF amplifier; (c)photonic link (including p-i-n photodiode)and transimpedance amplifier (TIA); (d) Photonic link with avalanche photodiode (APD) and integrated TIA. Here, the APD is modeled as a p-i-n photodiode (integral to the photonic link) followed by an avalanche current amplification process.

the cascaded noise figure is

$$NF_{total} = NF_1 + \sum_{n=2}^{N} \frac{NF_n - 1}{\prod_{j=1}^{n-1} G_j}, \tag{6b}$$

and the cascaded *OIP3* is given by

$$OIP3_{total} = \frac{OIP3_N}{1 + OIP3_N \left(\sum_{\substack{n=1 \\ N \geq 2}}^{N-1} \left[\left(OIP3_n \prod_{k=n+1}^{N} G_k \right) \right]^{-1} \right)} \quad . \tag{6c}$$

For the specific cases $N = 2$ and $N = 3$, we have

$$G = G_1 \cdot G_2 \tag{7a}$$

$$NF = NF_1 + \left(\frac{NF_2 - 1}{G_1} \right) \tag{7b}$$

$$OIP3 = \frac{OIP3_2}{1 + \frac{OIP3_2}{G_2} \left(\frac{1}{OIP3_1} \right)} \tag{7c}$$

and

$$G = G_1 \cdot G_2 \cdot G_3 \tag{8a}$$

$$NF = NF_1 + \left(\frac{NF_2 - 1}{G_1} + \frac{NF_3 - 1}{G_1 \cdot G_2} \right) \tag{8b}$$

$$OIP3 = \frac{OIP3_3}{1 + \frac{OIP3_3}{G_3} \left(\frac{1}{G_2 \cdot OIP3_1} + \frac{1}{OIP3_2} \right)} \tag{8c}$$

From Eqs (6a – 6c) and the that fact that all the quantities in these expressions are nonnegative, we see immediately the following general features of any cascaded series of RF gain elements:

1. Gains *anywhere* in the chain contribute to overall gain.
2. The noise figure of a chain can never be *smaller* than the NF of the *first* element in the chain.
3. The third-order intercept point of the chain can never be *larger* than the OIP3 of the *last* element in the chain.

Figures 4b, 4c and 4d show a combination of subsystems comprising the type of analog links we have in mind. Figure 4b shows a standard intensity-modulated link employing a p-i-n photodiode followed by an external RF amplifier; Fig. 4c shows a standard link employing a p-i-n diode followed by an external TIA; and Fig. 4d shows a standard link followed by an APD with an integrated TIA. In this last case, we assume that the APD can be represented as a p-i-n diode having responsivity equivalent to the responsivity of the APD at current gain $M = 1$ and followed by an avalanche current amplification process ($M > 1$).

For the systems shown in Fig. 4b or 4c, the overall (cascaded) system parameters become

$$G_{PL+G} = G_{PL} \cdot G_G \tag{9a}$$

$$NF_{PL+G} = NF_{PL} + \frac{NF_G - 1}{G_{PL}} \tag{9b}$$

$$OIP3_{PL+G} = \frac{OIP3_G}{1 + \frac{OIP3_G}{G_G}\left(\frac{1}{OIP3_{PL}}\right)} \tag{9c}$$

where the subscript “PL” denotes “photonic link” and the subscript “G” denotes “gain element” which, in these cases, means either an RF amplifier or a TIA.

For the system shown in Fig. 4d,

$$G_{PL+APD+TIA} = G_{PL} \cdot G_{APD} \cdot G_{TIA} \tag{10a}$$

$$NF_{PL+APD+TIA} = NF_{PL} + \frac{1}{G_{PL}}\left(NF_{APD} - 1 + \frac{NF_{TIA} - 1}{G_{APD}} \right) \tag{10b}$$

$$OIP3_{PL+APD+TIA} = \frac{OIP3_{TIA}}{1 + \frac{OIP3_{TIA}}{G_{TIA}}\left(\frac{1}{G_{APD} \cdot OIP3_{PL}} + \frac{1}{OIP3_{APD}} \right)} \tag{10c}$$

where the subscript "APD" denotes "avalanche photodiode."

When the received optical power is relatively low (<< 1mW), the photonic link portion of the overall gain will be very small $G_{PL} << 1$ and generally will be much smaller than the gain of either the TIA or the RF amplifier $G_{PL} << G_{RF}, G_{TIA}, G_{APD}$.

The RF gain of the TIA, derived in Appendix 2, is given by

$$G_{TIA} = \frac{R_{TIA}^2}{Z_o^2}. \tag{11}$$

where $R_{TIA}(V/A)$ is the transfer ratio or resistance of the TIA and *Z* is the external load resistance. The RF gain of the avalanche portion of the APD is given simply by

$$G_{APD} = M^2. \tag{12}$$

2.3 Noise

To complete this theory section we now present expressions for electrical noise power spectral densities for the systems under consideration. We make the simplifying assumption of neglecting laser intensity noise and optical amplifier noise. We also neglect non-thermal noise in the receiver electronics. At the output of the p-i-n

photodiode, the total electrical noise spectral density PSD_{noise} competing with the RF signal is

$$PSD_{noise,PL} = G_{PL}kT + kT + 2eI_{dc}Z/2^{2r} \tag{13}$$

The first term is the input thermal noise amplified by the photonic link gain, the second term is the thermal noise present in the output load independent of the presence of the link, and the third term is shot noise. By definition, the noise figure of the photonic link is the ratio of input to output signal-to-noise ratios

$$NF_{PL} = \frac{\frac{P_{RFsig}}{kT}}{\frac{G_{PL}P_{RFsig}}{G_{PL}kT + kT + 2eI_{dc}Z/2^{2r}}}$$

where P_{RFsig} is the RF signal power at the link input. Then

$$NF_{PL} = \frac{G_{PL}kT + kT + 2eI_{dc}Z/2^{2r}}{G_{PL}kT} = 1 + \frac{2^{1-2r}eI_{dc}Z}{G_{PL}kT} + \frac{1}{G_{PL}}. \tag{14}$$

Writing the link gain explicitly as a function of DC photocurrent, $G_{PL} = \left(g/2^{2r}\right)I_{DC}^2$, we have

$$NF_{PL} = 1 + \frac{2eZ}{gkT}I_{DC}^{-1} + \frac{2^{2r}}{g}I_{DC}^{-2} \equiv 1 + \alpha I_{DC}^{-1} + \beta I_{DC}^{-2} \tag{15}$$

where $\alpha = 2eZ/gkT$ and $\beta = 2^{2r}/g$. Figure 5 shows the noise figure as a function of DC photocurrent for the two cases *r = 0* (no internal load resistor) and *r = 1* (internal resistor). The noise figure for the r = *0* case is 6 dB better than the *r = 1* case at low photocurrents where the term proportional to I_{DC}^2 dominates. From an RF link

perspective, the values of noise figure over the range of photocurrents shown in Fig. 5 – corresponding to typical expected values of received optical power – are quite poor. This plot indicates quite strikingly that any useful employment of a free-space link for analog signal transmission will be limited to photocurrents above, say, 10 uA. Otherwise, the motivation for using an intensity-modulated, direct-detection (IMDD) analog link over a long free-space must be sufficiently high to accept the exceedingly poor noise figure. We hasten to add that other analog modulation/demodulation techniques may offer performance superior to IMDD but, in any case, very low photocurrent values will always yield poor analog link performance.

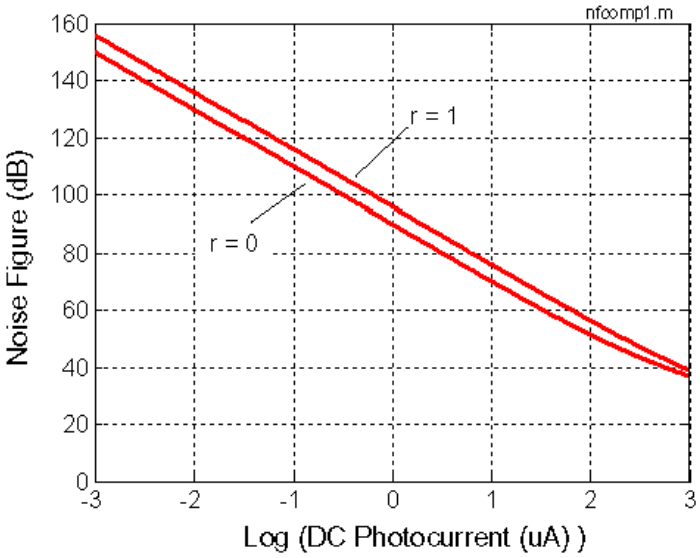

Fig. 5. Noise figure of an analog IMDD photonic link as a function of DC photocurrent for the two cases r = 0 (no internal load resistor) and r = 1 (internal load resistor).

We now calculate the noise figure of the APD. We assume that the excess noise factor of the APD can be written $F = M^x$ [Gowa84, Gagl95, Alex97] where the exponent *x* lies in the range 0.2 to 1.0. Again, for simplicity, we neglect laser intensity noise. Then the power in the RF signal entering the APD is $S_{in} = G_{PL} P_{RF,in}$ and the RF power exiting the APD is $S_{out} = M^2 G_{PL} P_{RF,in}$. The electrical noise power spectral

density at the APD input (photonic link output) contains both amplified thermal noise and shot noise, $PSD_{noise,in} = G_{PL}kT + 2eI_{DC}Z_o$. We do not include here the kT term for output thermal noise because the avalanche gain process occurs directly in the photodetector itself. Also, the expression for shot noise assumes no internal load resistor is present, again, because the avalanche gain is internal to the photodetector. At the APD output the noise is $PSD_{noise,out} = M^2\left[G_{PL}kT + 2M^x eI_{DC}Z_o\right] + kT$. Hence, the noise factor of the APD becomes

$$NF_{APD} = \frac{\dfrac{G_{PL}P_{RF,in}}{G_{PL}kT + 2eI_{DC}Z_o}}{\dfrac{M^2 G_{PL}P_{RF,in}}{M^2\left[G_{PL}kT + 2M^x eI_{DC}Z_o\right] + kT}}.$$

Simplifying,

$$NF_{APD} = \frac{\left(M^2 G_{PL} + 1\right)kT + 2M^{2+x}eI_{DC}Z_o}{M^2\left(G_{PL}kT + 2eI_{DC}Z_o\right)}. \tag{16}$$

Since $G_{PL} = gI_{DC}^2$ where $g = Z_i Z_o\left(\pi/V_\pi\right)^2$, the noise factor can be written as a ratio of quadratic functions of DC photocurrent

$$NF_{APD} = \frac{aI_{DC}^2 + bI_{DC} + c}{aI_{DC}^2 + dI_{DC}} \tag{17}$$

where $a = gM^2kT$, $b = 2M^{2+x}eZ_o$, $c = kT$, and $d = 2M^2 eZ_o$.

Figure 6 shows NF_{APD} as a function of I_{DC} for $x = 0.2 \& 1.0$ and $M = 10 \& 100$. For these plots we assumed $Z_i = Z_o = 50$ ohms, $V_\pi = 5.6$ Volts, and $T = 298$ K.

A comparison of Figures 5 and 6 shows that, over the entire range of photocurrents of interest, $NF_{APD} << NF_{PL}$. Furthermore, the noise figure of a high-quality RF amplifier is usually on the order of or less than a few dB and, for narrowband amplifiers, can easily be less than 1 dB. Hence, the *NF* of the APD will generally be larger than the *NF* of a corresponding RF amplifier except possibly in the regime of moderate *M*, low *x*, and large received optical power.

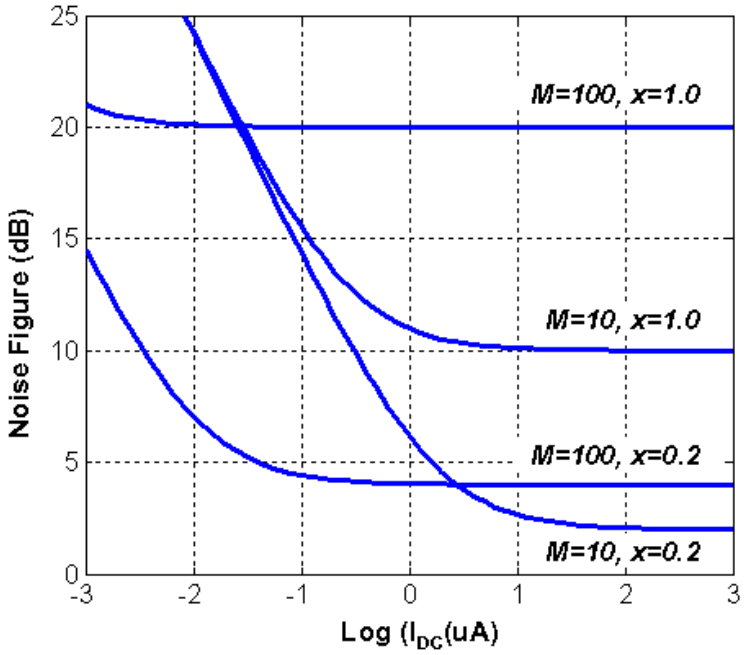

Fig. 6. Noise figure NF_{APD} of the APD as a function of DC photocurrent at the photonic link output for APD parameter values M = 10,100 and for x = 0.2,1.0.

3. Experimental Results

We preformed a series of laboratory experiments using an optical fiber link, as shown in Fig. 7, to confirm the validity of the theory developed in Section 2. The link comprised a distributed feedback laser (DFB) (Alcatel 3CN00302CM) operating near 1.55 um wavelength, an external Mach-Zehnder modulator (MZM) (JDS Uniphase 10020462), approximately two meters of singlemode fiber, a fiber-pigtailed, manually-controlled optical attenuator (OZ Optics), a 50:50 fused fiber coupler, an optical power meter (Newport 1835-C w/Model 818-IS-1 Universal Fiber Optic Detector), and a photoreceiver. The RF source (Agilent E8267C PSG Vector Signal Generator (VSG)) provided two tones near 1 GHz and separated by 1.33 MHz to the MZM. The electrical bandpass filter (K&L 3C45-1000/T2-0/0) strongly attenuated any intermodulation or harmonic signals originating in the RF source itself from reaching the

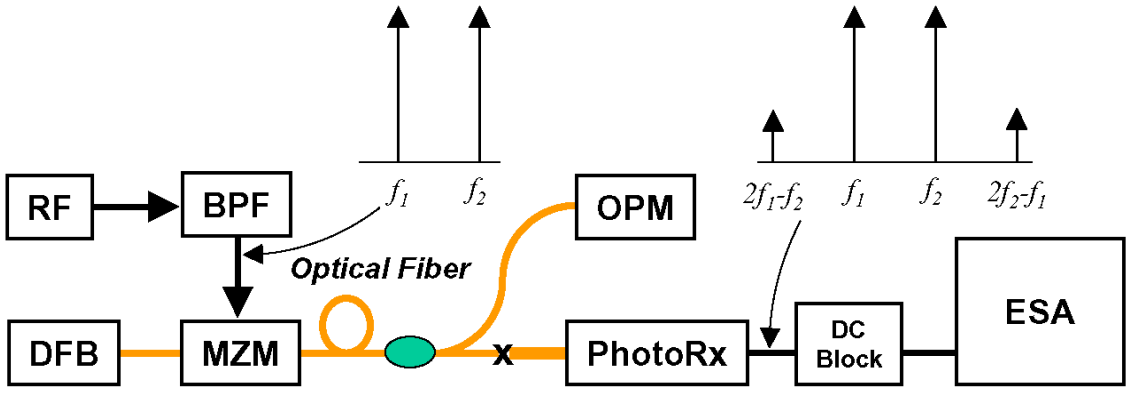

Fig. 7. Set-up for laboratory measurements including distributed feedback laser (DFB), Mach-Zehnder electro-optical modulator (MZM), RF source (RF), electrical band-pass filter (BPF), optical power meter (OPM), photoreceiver (PhotoRx), and electrical spectrum analyzer (ESA). The optical link in this case consisted of a few meters of singlemode (SM) optical fiber. The "x" indicates the location of a splice between SM fiber and multimode fiber pigtailed to the photodiode in the photoreceiver (for the case of the receiver configuration (c) shown below in Fig. 8).

MZM. An electrical spectrum analyzer (Agilent 8563EC) was used to record the RF spectrum of the photoreceiver output. As shown in Fig. 8, three photoreceivers

configurations were investigated 1) a p-i-n photodiode with built-in 50 ohm resistor (Discovery Semiconductor DSC30S pigtailed with 62.5/125 multimode fiber); 2) the same p-i-n photodiode with an external RF amplifier (Miteq AM-4A-0510 (500-1000MHz)); and 3) a p-i-n photodiode with an integrated TIA amplifier (Discovery Semiconductor DSC-R402AC-73-FC/UPC-K-1).

A summary of the RF parameters (including parameters measured in this study) for the RF amplifier and the transimpedance amplifier is given in Appendix 3.

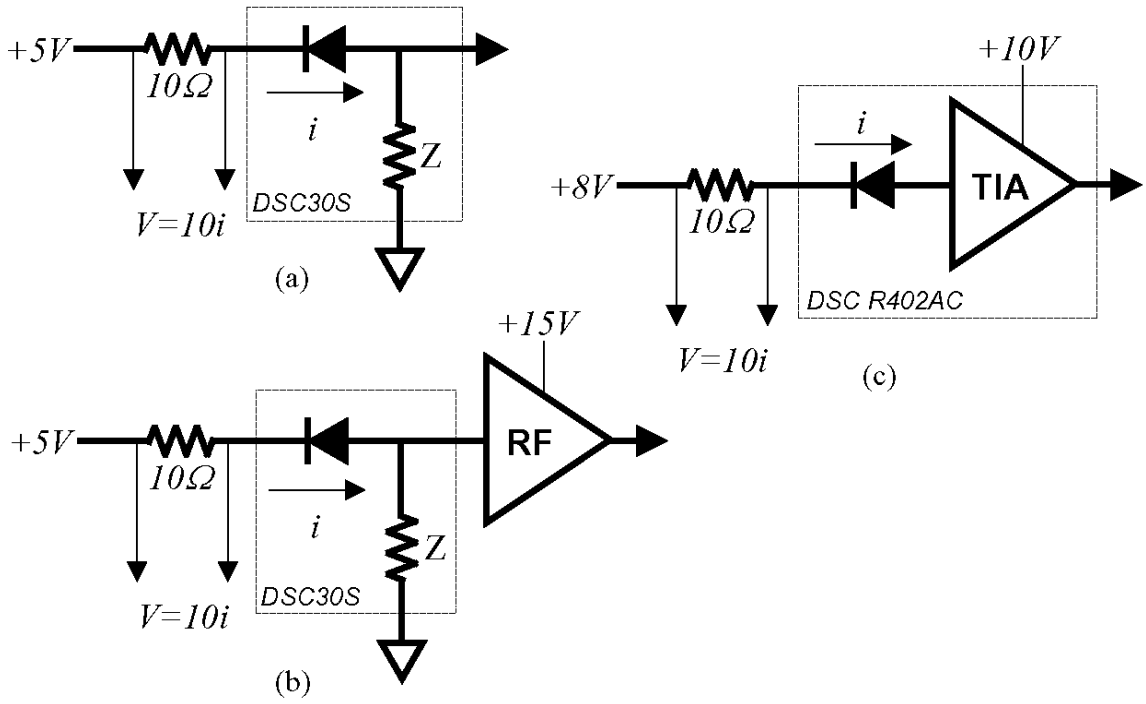

Fig. 8. The three photoreceiver configurations studied: (a) photodiode with integrated load resistor; (b) photodiode with integrated load resistor and external RF amplifier; and (c) photodiode with integrated TIA.

3.1 Source Calibration

For the two-tone measurements performed in this investigation, the Agilent VSG was run with the following settings: *Mode* = Two-Tone, *Freq Sep* = 1.33 MHz, *Alignment* = Center. The power in each signal entering the MZM was calibrated against the RF power setting on the VSG. The results are shown graphically in Fig 9. The center frequency (1000.112 MHz) of the tones was chosen to be symmetrically disposed with respect to the passband of the BPF and the frequency separation (1.33 MHz) was chosen arbitrarily to be an unambiguously identifiable value. For completeness, Figure 10 shows the residual (post-BPF) high-frequency intermodulation spur as a function of the RF power in the higher-frequency tone. These levels are low enough to properly measure the intermodulation distortion of the optical system.

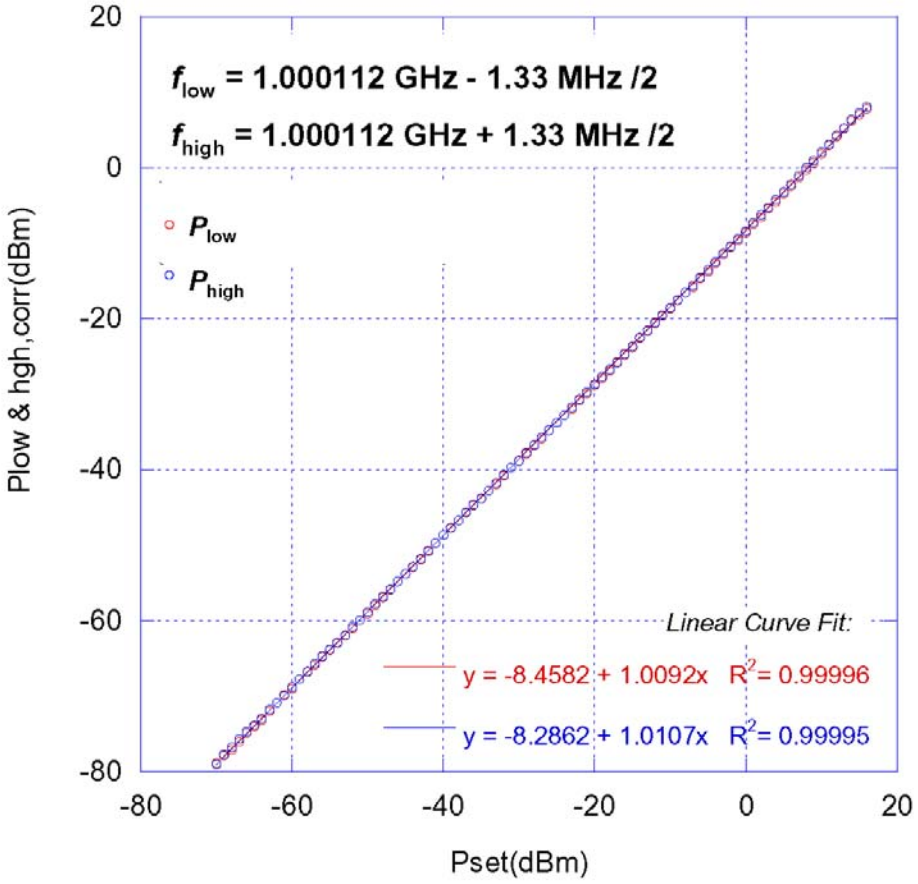

Fig. 9. Calibration curves for RF power (dBm) in each tone of the two-tone CW output as a function of the power setting (dBm) on the VSG.

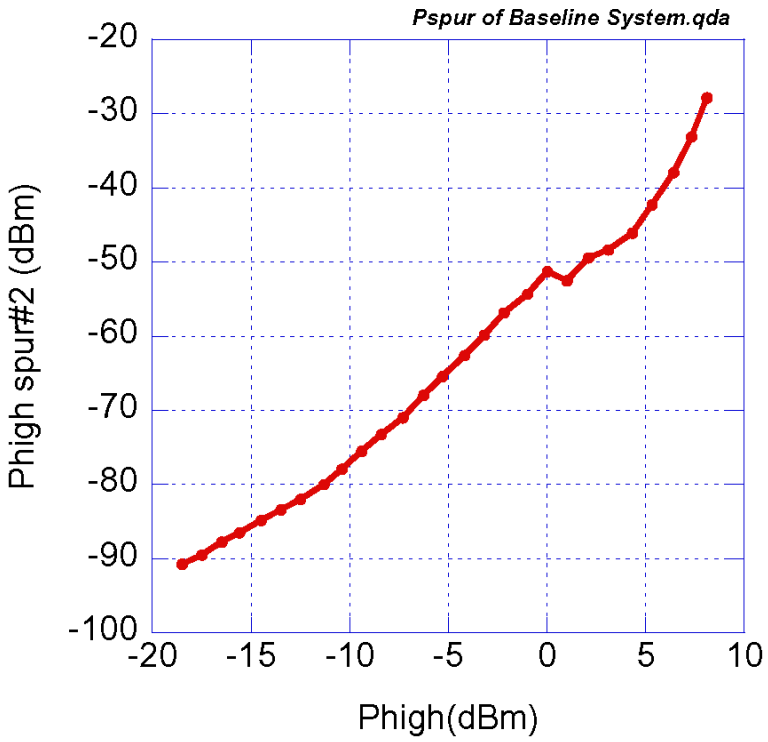

Fig. 10. Residual intermodulation distortion (high-frequency IMD spur) of the signal entering the MZM.

Next, the RF properties of the Miteq amplifier were measured. Figure 11a shows the output power in the two-tone fundamentals and intermodulation tones as a function of RF power applied to the MZM. The third-order output intercept point obtained in the standard fashion using the graph itself is estimated to be OIP3 = +23.7 dBm, as shown. The upper curve of Figure 11b shows that the RF gain as a function of RF power applied to the MZM is approximately +56 dB in the linear regime with compression beginning near – 48 dBm input power. The lower curve in Fig. 11b shows the OIP3 calculated using the expression [Uric09]

$$\mathrm{OIP3} = \left(P_{f1,2}^{3} \Big/ P_{(2f_1 - f_2)} \right)^{1/2}$$

where $P_{f_{1,2}}$ is the power in either tone (assuming the tones have equal power) and $P_{(2f_1-f_2)}$ is the power in either spur. Note that *OIP3* obtained in this fashion is in close agreement with the *OIP3* value obtained using traditional graphical analysis. (Fig 11a)

3.2 Measurement Technique

Here we discuss briefly the RF measurement technique used with the electrical spectrum analyzer (ESA). Measurements were performed in either of two modes: 1)“narrowband” with a 2 MHz span, or 2) “wideband” with a 5 MHz span. Wideband measurements allowed simultaneous recording of all four signals: low-frequency spur, low-frequency tone, high-frequency tone, and high-frequency spur. The amplitude scale typically used was 10 dB/div. To obtain better power accuracy, the narrowband measurements were performed for one spur at a time with 2dB/div scale. At each input power level, the ESA reference level was manually adjusted to bring the measured power in the strongest signal to within 2-4 dB of the top of the trace. Video averaging was used, typically 8-64 averages, depending on how close the signal was to the noise floor.

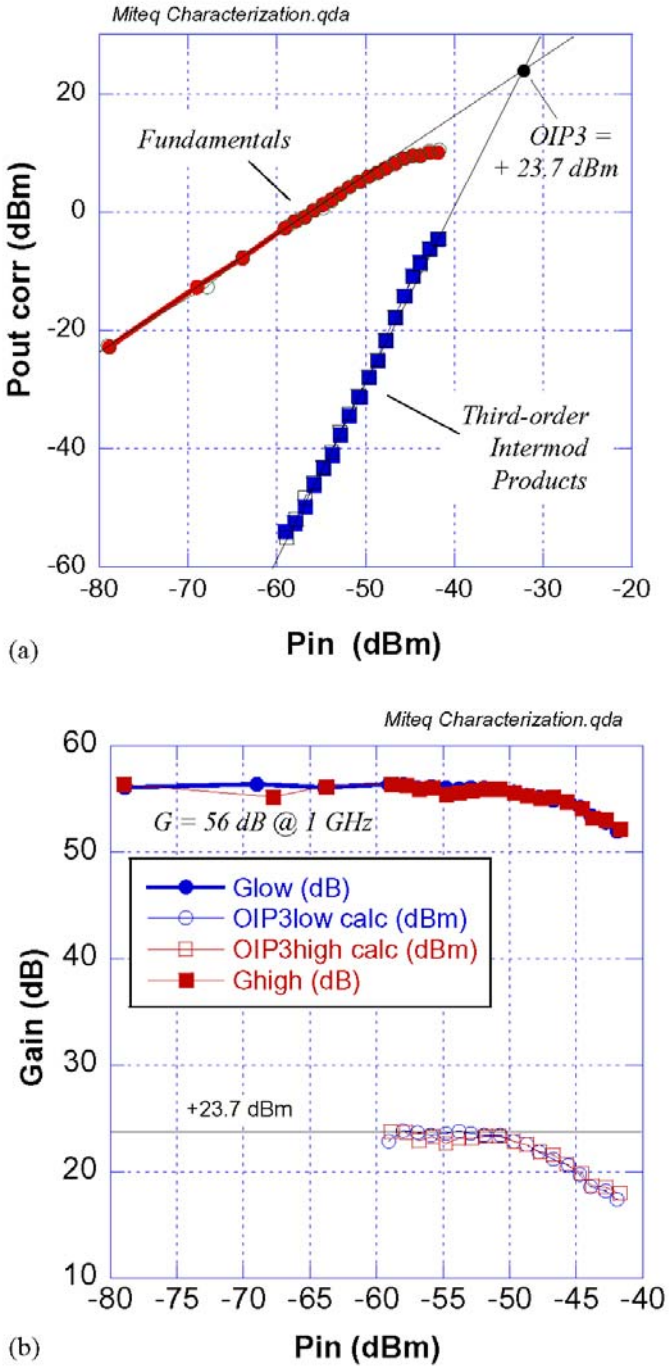

Fig. 11. (a) Power in fundamental and intermodulation tones as a function of input RF power in each tone applied to the MZM. By this graphical analysis, we find OIP3 ~ +23.7 dBm. (b) RF Gain and OIP3 (lower curve, calculated using Eq (4) with r = 1) as a function of applied RF power.

3.3 Photonic Link

Next, the RF parameters of the photonic link itself (no post-amplification) were measured. Here the DSC30S photodetector was used. The results for RF gain are shown in Fig. 12. The validity of the analog optical link equations (summarized in Appendix 1) is by now so well established that we can use the equations to experimentally determine V_π of the modulator near 1 GHz. Since the DSC30S contains an internal 50 ohm load resistor we use

$$G(dB) = -22 + 20\log I_{dc}(mA) - 20\log V_\pi(V)\,.$$

Then, since $G = -37.8\ dB$ and $I_{dc} = 0.9\ mA$, we find $V_\pi = 5.6\ V\ @1\ GHz$.

For this same link it is difficult to measure the noise figure directly. At 1 mA DC photocurrent, thermal and shot noise each contribute –174 dBm/Hz (with the DSC30S) leading to a total expected noise power spectral density of –172.5 dBm/Hz (i.e. resulting from the incoherent summation of the two noise sources.) If these were the only sources of noise the expected noise figure would be found using (Appendix 1)

$$NF(dB) = PSD_{noise}(dBm/Hz) - G(dB) + 174 dBm/Hz$$

or $NF = -172.5 - (-37.8) + 174 = 39.3\ dB$. We measured a noise floor of -102 dBm / 30 kHz = -146.8 dBm / Hz. We did not independently measure the contribution of laser RIN to the noise floor. However, by terminating the input to the ESA in 50 ohms, we verified that the -146.8 dBm/Hz noise floor was due to the ESA itself. (The proper way to measure *NF* in this case is to add a low-noise RF amplifier, having known *NF*, to the system output – but this is exactly the overall system shown in Fig. 8b – a configuration to be discussed below.)

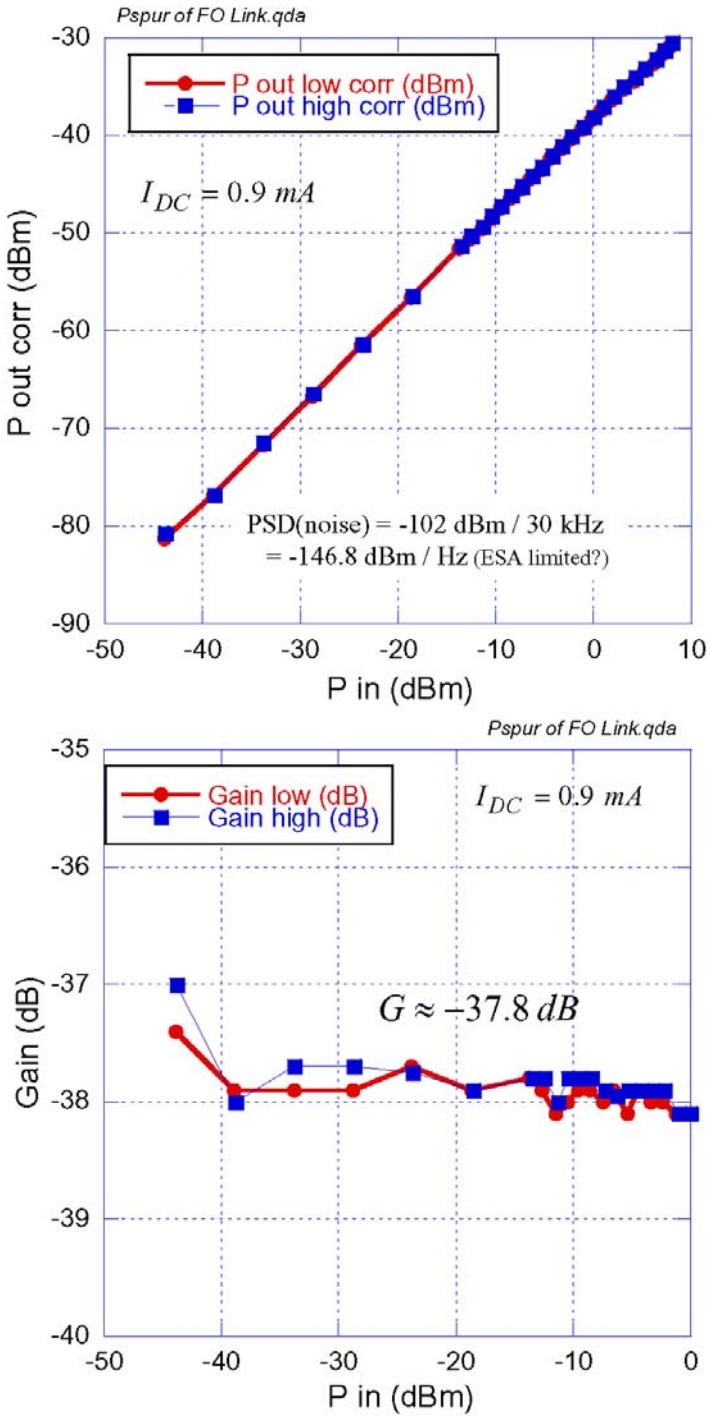

Fig.12. RF gain measurement for the "bare" optical link. (a) Output power in each tone as a function of input power. (b) RF Gain in each tone as a function of input power.

Next, we measured OIP3. The results are summarized in Fig. 13. Theory predicts the value $OIP3_{imd}\,(dBm) = -43 + 20\log I_{dc}\,(\mathrm{mA})$ or $OIP3_{imd} = -14.0\ dBm$. Standard graphical analysis yielded values in the range $OIP3_{imd} = -15.2$ to $-15.9\ dBm$. The *OIP3* values obtained at each power level using the above expression fall roughly in between the theory and graphical values (although there is no *a priori* reason to expect this to be true in general). Data points in Fig. 13 labeled "full" were obtained using the

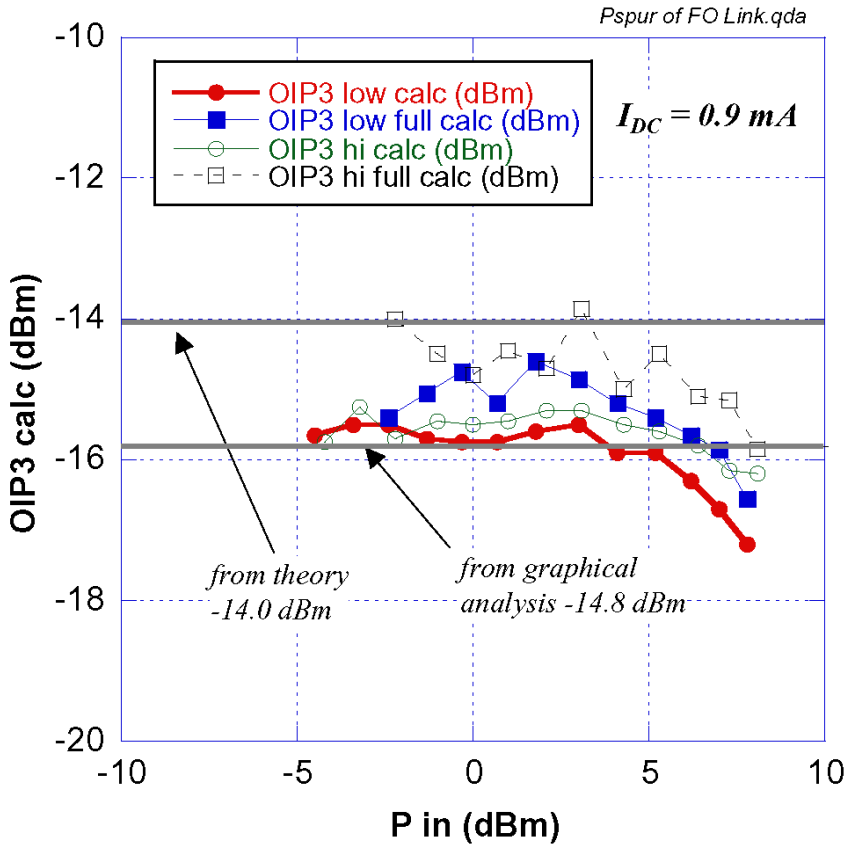

Fig.13. Measured OIP3 for the photonic link. The designation "full" indicates the data used to calculate OIP3 were obtained from wideband measurements. The straight line labeled "from theory" corresponds to the value calculated using the value of I_{DC} *and Eq. (4) with r = 1, while the straight line labeled "from graphical analysis" corresponds to the value obtained from traditional analysis of the intercept between fundamental and third-order intermodulation responses.*

5 MHz span, while the other points were obtained using the 2 MHz span. Slight discrepancies between theory and observation may arise here due to slight inequalities between the power in the two applied tones since the theory assumes the tone powers are exactly matched. Another possible source of discrepancy is the nonlinear response of the photodiode itself [Hast09].

3.4 RF-Amplified Photonic Link

In this section we report the results of measurements made after adding an RF amplifier to the link output (Fig. 8b) and repeating measurements of gain, noise figure and OIP3. For these measurements the DC photocurrent was reduced to $I_{DC} = 92\mu A$ by adjusting the manual optical attenuator. The results for gain and OIP3 are shown in Fig. 14.

The expected gain is calculated simply as the sum of the (calculated) link gain at 92 uA photocurrent, – 57.9 dB, and the +56 dB gain of the RF amplifier, leading to an overall gain of –1.9 dB in good agreement with the observed value of approximately –2.3 dB.

To determine the expected overall OIP3 we use the cascaded OIP3 formula (Eq 9c)

$$OIP3 = \frac{OIP3_{RF}}{1 + \frac{OIP3_{RF}}{G_{RF} \cdot OIP3_{PL}}}$$

We estimate the OIP3 of the link for $I_{DC} = 92\mu A$ using the expression $OIP3_{PL} \approx I_{DC}^2 Z = -33.7\ dBm$. Then, with the values $G_{RF} = +56dB$ and $OIP3_{RF} = +23.7dBm$ we calculate $OIP3 = +19.9dBm$ in good agreement with the measured value slightly below $OIP3 = +19\ dBm$.

Finally, the measured noise floor was -76.5 dBm in 10 kHz RBW or –116.5 dBm/Hz leading to a calculated noise figure

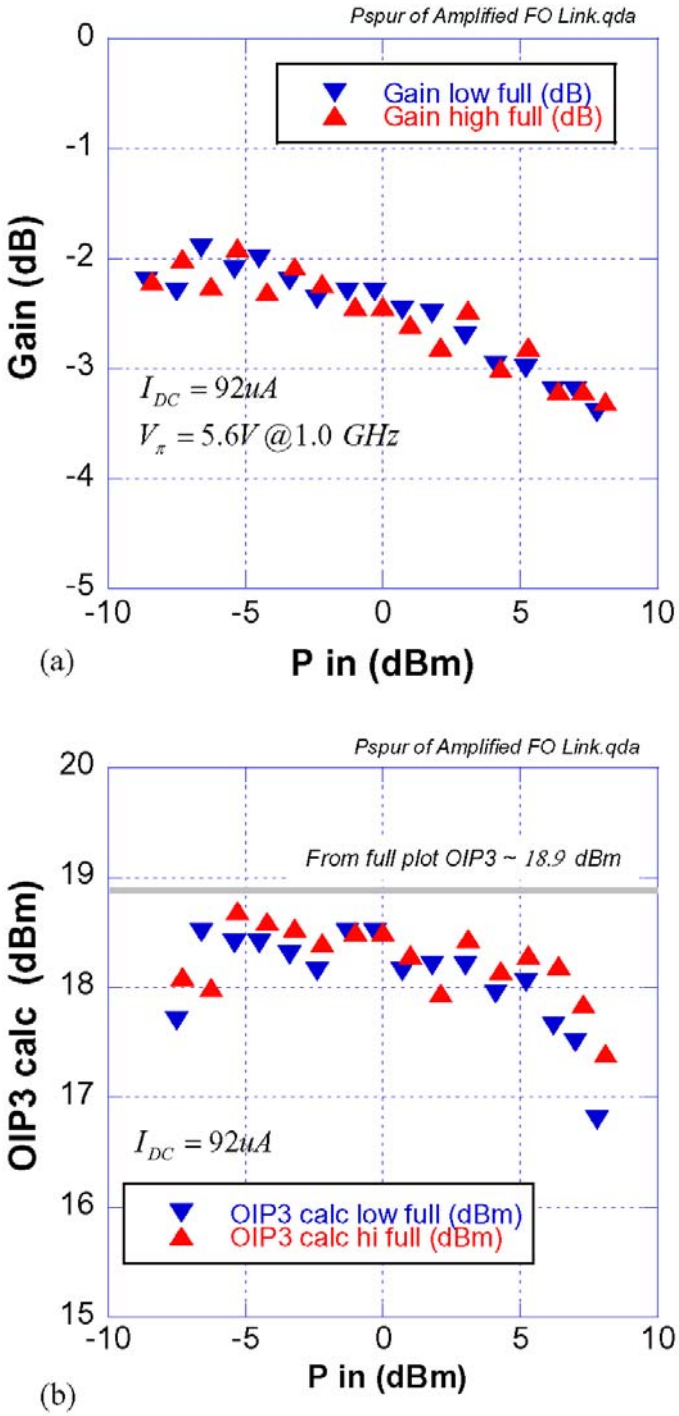

Fig. 14. Measured Gain and OIP3 for the RF-amplified link

$NF(dB) = PSD_{noise}(dBm/Hz) - G(dB) + 174$ or $NF = +59.7dB$. This poor noise figure is not unexpected since the first element in the cascade of gain elements, namely the photonic link, has such a poor noise figure itself due to the low received photocurrent.

3.5 TIA-Amplified Photonic Link

Finally, we investigated a link employing a transimpedance amplifier integrated with a pin photodiode (DSC-R402AC-73-FC/UPC-K-1) as shown in Fig. 8c. For these measurements the dc photocurrent was 100 uA obtained by manually adjusting the optical attenuator. The results for gain and *OIP3* are shown in Fig. 15.

The expected gain is calculated again as the product of the link gain at 100 uA photocurrent, –51.9 dB , (calculated using the gain expression (Appendix 1) without an internal load resistor) and the +21.6 dB gain of the TIA amplifier, leading to an overall calculated gain of –30.3 dB, a value in good agreement with the observed value of approximately –29.7 dB.

We measured *OIP3* to be – 6.9 dBm using graphical analysis, and we calculate *OIP3* to be in the range –7.1 dBm to –7.8 dBm using Eq (4) with $r = 0$. Unfortunately, we do not have manufacturer's test data for *OIP3* for this particular photoreceiver, other than a nominal value of +37 dBm for this class of receiver. If we use this nominal OIP3 value, employ the cascaded *OIP3* formula

$$OIP3 = \frac{OIP3_{TIA}}{1 + \frac{OIP3_{TIA}}{G_{TIA} \cdot OIP3_{PL}}},$$

assume the link *OIP3* is given by $OIP3_{PL} = 4I_{DC}^2 Z$ and that $I_{DC} = 100\ uA$ and $OIP3_{PL} = -27\ dBm$, then we calculate *OIP3 = –5.4 dBm* – a value remarkably close to the measured value considering the uncertainty in the value of $OIP3_{TIA}$.

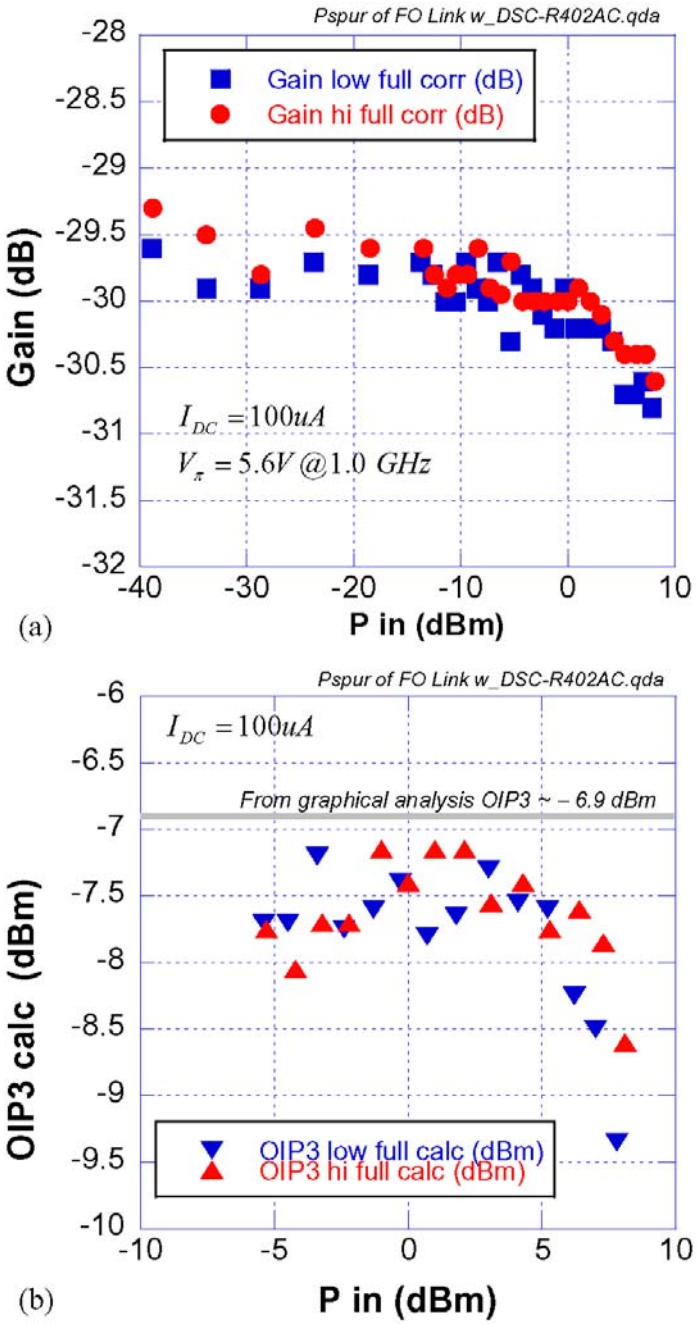

Fig. 15. Measured Gain and OIP3 for the TIA-amplified link

In order to measure the output noise power spectral density for this system we needed to use the Miteq RF amplifier (G = +56 dB, NF = 1.6 dB) on the output. With this arrangement we measured a noise floor of –56.6 dBm / 30 kHz = -101.4 dBm / Hz. After correcting for the gain and noise figure of the Miteq amplifier we find a corrected noise power spectral density $PSD_{noise}(dBm/Hz) = -101.4dBm - 56 - 1.6 = -159\ dBm/Hz$. From this value we calculate the noise figure, assuming *G = –30 dB:*

$NF(dB) = PSD_{noise}(dBm/Hz) - G(dB) + 174$ or $NF = +\ 45\ dB$.

4. Comparison of Architectures

In this final section we compare the theoretical RF performance of the two system architectures shown in Figs 4b or 4c and 4d, namely, a p-i-n photodiode followed by an amplifier; and an avalanche photodiode (APD) followed by an amplifier.

We need to make one careful distinction between the assumed form of the p-i-n photodiode in the two cases. For practical purposes, the p-i-n diode in architecture 4b or 4c will likely be integrated into a package containing an internal load resistor for frequency flattening. Hence, the equations in Appendix 1 corresponding to *r = 1* apply in this case. For the architecture in Fig 4d, on the other hand, the model for the APD does not include an internal load resistor since the current gain is integrated in the photodiode itself. Hence, the *r = 0* equations in Appendix 1 apply here.

To make a fair comparison, we assume that G_{PL} is the same in both cases and that the overall post-photonic link gains are equal, that is, $G_G = G_{APD} \cdot G_{TIA}$.

To compare noise figures we use Eqs 9b and 10b, and form the ratio

$$\frac{NF_{PL+APD+TIA}}{NF_{PL+G}} = \frac{NF_{PL} + \frac{1}{G_{PL}}\left(NF_{APD} - 1 + \frac{NF_{TIA} - 1}{G_{APD}}\right)}{NF_{PL} + \frac{1}{G_{PL}}\left(NF_G - 1\right)}$$

In general, $G_{APD} = M^2 >> 1$ and, for moderate to long distance FSO links, it will also be true that $G_{PL} << 1$ and $NF_{PL} >> 1$. With these approximations, the above equation becomes

$$\frac{NF_{PL+APD+TIA}}{NF_{PL+G}} \approx \frac{NF_{APD}}{NF_G} \tag{18}$$

The noise figure for a broad-band, low-noise RF amplifier is often less than 3 dB and, for a narrow-band, low-noise RF amplifier, the noise figure often approaches 1 dB. From Fig. 6 it is seen that the noise figure of the APD is much greater than one over the range of expected DC photocurrents. Hence, ***to optimize the overall link noise figure, it is preferable to use a p-i-n photodiode followed by a high-quality RF amplifier rather than an APD followed by a TIA amplifier (or any electrical amplifier).***

We now compare the third-order output intercept points. Using Eqs 9c and 10c we form the ratio $OIP3_{PL+G} / OIP3_{PL+APD+TIA}$ where, recall,

$$OIP3_{PL+G} = \frac{OIP3_G}{1 + OIP3_G \left(\dfrac{1}{G_G \cdot OIP3_{PL}} \right)} \tag{19}$$

and

$$OIP3_{PL+APD+TIA} = \frac{OIP3_{TIA}}{1 + OIP3_{TIA} \left(\dfrac{1}{G_{TIA} \cdot G_{APD} \cdot OIP3_{PL}} + \dfrac{1}{G_{TIA} \cdot OIP3_{APD}} \right)}. \tag{20}$$

The ratio is

$$\frac{OIP3_{PL+G}}{OIP3_{PL+APD+TIA}} = \frac{OIP3_G}{OIP3_{TIA}} \frac{1+\frac{OIP3_{TIA}}{G_{TIA}}\left(\frac{1}{G_{APD}\cdot OIP3_{PL}}+\frac{1}{OIP3_{APD}}\right)}{1+\frac{OIP3_G}{G_G}\left(\frac{1}{OIP3_{PL}}\right)} \tag{21}$$

Making approximations to simplify this expression is not as straightforward as it was for the noise figure, and an evaluation of the ratio can be made, in general, only after specific values of the relevant parameters are known for specific systems. However, if it were true that the received optical power was so low that $G_{APD}\cdot OIP3_{PL} << OIP3_{APD}$, then we could write

$$\frac{OIP3_{PL+G}}{OIP3_{PL+APD+TIA}} \approx \frac{OIP3_G}{OIP3_{TIA}} \frac{1+\frac{OIP3_{TIA}}{G_{TIA}}\left(\frac{1}{G_{APD}\cdot OIP3_{PL}}\right)}{1+\frac{OIP3_G}{G_G}\left(\frac{1}{OIP3_{PL}}\right)} \tag{22}$$

Since we want the comparison to be made under the normalizing condition $G_G = G_{APD}\cdot G_{TIA}$, we have

$$\frac{OIP3_{PL+G}}{OIP3_{PL+APD+TIA}} \approx \frac{OIP3_G}{OIP3_{TIA}}, \tag{23}$$

For commercially-available RF amplifiers and transimpedance amplifiers, it will generally be true that $OIP3_{TIA} < OIP3_G$. Hence, under the assumption $G_{APD}\cdot OIP3_{PL} << OIP3_{APD}$, ***to optimize the overall link OIP3,and under the assumption that the product of the APD gain and the OIP3 of the photonic link is much smaller than the OIP3 of the APD, it is preferable to use a p-i-n photodiode followed by a high-quality RF amplifier rather than an APD followed by a TIA amplifier (or any electrical amplifier).***

5. Summary

Our goal in this report was to compare the radio-frequency (RF) performance of various photodetection architectures for use in free-space analog photonic links in order to understand how to optimize overall link performance at microwave frequencies. The discussion and experiments were limited to intensity-modulated, direct-detection photonic links.

We presented the basic theory for an RF link employing a photonic segment. We conducted experiments comparing three photoreceiver architectures: 1) a p-i-n photodiode with internal load resistor; 2) a p-i-n photodiode with internal load resistor followed by a high-gain, RF electrical amplifier; and 3) a p-i-n diode followed by a transimpedance amplifier. In all cases, the experimental results agreed closely with the predictions of theory.

Finally, we derived expressions to predict the performance of a photoreceiver comprising an avalanche photodiode (APD) followed by an RF gain element (either a TIA or an RF amplifier. Typically, an APD is employed to provide gain internal to the photodiode and thus relieve the performance requirements for any external amplifier. By comparing the RF link metrics of gain, noise figure, and linearity for these various architectures, we assessed the utility of the two approaches.

We conclude that an architecture comprising a p-i-n diode, with or without an internal load resistor, followed by a high-quality, high-gain RF amplifier is almost always the preferred receiver architecture.

6. References

Uric09	V.J. Urick, J. Diehl, A. Hastings, C. Sunderman, J.D. McKinney, P.S. Devgan, J.L. Dexter and K.J. Williams, **"Analysis of fiber-optic links for HF antenna remoting,"** *NRL Technical Memorandum Report NRL/MR/5650—09-YYYY*
Buch08	F. Bucholtz, V.J. Urick, M. Godinez and K.J. Williams, **"Graphical approach for evaluating performance limitations in externally modulated analog photonic links,"** *IEEE Trans. Micro. Theory Techn.* ***56****(1) 242-247 (2008).*
Buch09	F. Bucholtz , H.R. Burris, C.I. Moore, C. S. McDermitt, R. Mahon, M. R. Suite, G. C. Gilbreath and W.S. Rabinovich, "**Statistical Properties of a Short, Analog RF Free-Space Optical Link,"** *Proc. SPIE* ***7324****, 73240D (2009)*
Burr09	H.R. Burris, F. Bucholtz , C.I. Moore, Kenneth J. Grant, M.R. Suite, C. S. McDermitt, B.A. Clare, R. Mahon, W. Martinsen, M. Ferraro, R. Sawday, C. O. Font, L. M. Wasiczko Thomas,K. A. Mudge, W.S. Rabinovich G. C. Gilbreath, W. Scharpf, E. Saint Georges and S. Uecke, "**Long-range analog RF free-space optical comm link in a maritime environment,"** *Proc. SPIE* ***7324****, 73240G (2009)*
Gowa84	J. Gowar, **Optical Communication Systems**, Prentice-Hall, 1984.
Gagl95	R. M. Gagliardi and S. Karp, **Optical Communications**, Wiley, New York, 1995.
Alex97	S. B. Alexander, **Optical Communication Receiver Design**, SPIE Optical Engineering Volume TT22, 1997.
Hast09	A.S. Hastings, D. A. Tulchinsky and K.J. Williams, **"Photodetector nonlinearities due to voltage-dependent responsivity,"** Photon. Technol. Lett., **21** (21) 1642-1644 (2009).

Appendix 1: Summary of Equations for RF Analog IMDD Link with MZM at Quadrature

$G=\left(\frac{\pi}{2^r}\right)^2\left(\frac{I_{dc}}{V_\pi}\right)^2 Z_{in}Z_{out}$ where $\begin{cases} r=0 & \text{w/o 50 }\Omega \\ r=1 & \text{w/ 50}\Omega \end{cases}$	$G(dB)=$ $\begin{cases} -16+20\log\left(I_{dc}(mA)\right)-20\log\left(V_\pi(V)\right) & \text{w/o 50}\Omega \\ -22+20\log\left(I_{dc}(mA)\right)-20\log\left(V_\pi(V)\right) & \text{w/ 50}\Omega \end{cases}$
$NF=\left(\frac{PSD_{noise}(W/Hz)}{GkT}\right)$ $=\left(\frac{2^r}{\pi}\right)^2\left(\frac{V_\pi}{I_{dc}}\right)^2\frac{PSD_{noise}(W/Hz)}{Z_{in}Z_{out}}$	$NF(dB)$ $=PSD_{noise}(dBm/Hz)-G(dB)+174$ $=PSD_{noise}(dBm/Hz)+20\log\left(V_\pi\right)-20\log\left(I_{dc}\right)+\left(6r-44\right)$
$OIP3_{imd}=\begin{cases} 4I_{dc}^2Z_{out} & \text{w/o 50}\Omega \\ I_{dc}^2Z_{out} & \text{w/ 50}\Omega \end{cases}$ $OIP3_{3h}=\begin{cases} 12I_{dc}^2Z_{out} & \text{w/o 50}\Omega \\ 3I_{dc}^2Z_{out} & \text{w/ 50}\Omega \end{cases}$	$OIP3_{imd}(dBm)=\begin{cases} -37+20\log I_{dc}(\text{mA}) & \text{w/o 50}\Omega \\ -43+20\log I_{dc}(\text{mA}) & \text{w/ 50}\Omega \end{cases}$ $OIP3_{3h}(dBm)=\begin{cases} -32.2+20\log I_{dc}(\text{mA}) & \text{w/o 50}\Omega \\ -38.2+20\log I_{dc}(\text{mA}) & \text{w/ 50}\Omega \end{cases}$
$\text{OIP3}_{imd}=\left(P_{f_{1,2}}^3/P_{(2f_1-f_2)}\right)^{1/2}$ $\text{OIP3}_{3h}=\left(P_f^3/P_{3f}\right)^{1/2}$ $\text{OIP3}_{3h}=3\bullet\text{OIP3}_{imd}$	
$OIP3_{imd}=\left(\frac{4}{\pi^2}\frac{V_\pi^2}{Z_{in}}\right)G\ \begin{cases} \text{w/ or} \\ \text{w/o 50}\Omega \end{cases}$ $OIP3_{3h}=\left(\frac{12}{\pi^2}\frac{V_\pi^2}{Z_{in}}\right)\text{G}\ \begin{cases} \text{w/ or} \\ \text{w/o 50}\Omega \end{cases}$	$OIP3_{imd}(dBm)\doteq 9+20\log(V_\pi)+G(dB)\ \begin{cases} \text{w/ or} \\ \text{w/o 50}\Omega \end{cases}$ $OIP3_{3h}(dBm)\doteq 15+20\log(V_\pi)+G(dB)\ \begin{cases} \text{w/ or} \\ \text{w/o 50}\Omega \end{cases}$
$SFDR3_{imd}=\left(OIP3_{imd}/PSD_{noise}\right)^{2/3}$	$SFDR3\left(dB\cdot Hz^{2/3}\right)=$ $(2/3)\left[OIP3_{imd}(dBm)-PSD_{noise}(dBm/Hz)\right]$
$NF\bullet SFDR3_{imd}^{3/2}(Hz)=\frac{4\left(V_\pi/\pi\right)^2}{kTZ_{in}}$ $G\bullet NF\bullet SFDR3_{imd}^{3/2}(Hz)=\frac{OIP3_{imd}}{kT}$	

$$NF \bullet SFDR3_{imd}^{3/2}(Hz) = \frac{4\left(V_\pi/\pi\right)^2}{kTZ_{in}}$$

$$G \bullet NF \bullet SFDR3_{imd}^{3/2}(Hz) = \frac{OIP3_{imd}}{kT}$$

$$PSD_{shot} = 2eI_{dc}Z_{out}/2^{2r}$$

where $\begin{cases} r = 0 \text{ No internal } \Omega \\ r = 1 \text{ Internal } 50\Omega \end{cases}$

$$PSD_{shot}(dBm/Hz) = -168 - 10\log(I_{dc}) - 6x$$

$$At\ I_{dc} = 1mA,\ PSD_{shot} = -168 - 6x$$

$$PSD_{thermal} = kT@290K$$
$$= 4\times10^{-21}\ W/Hz$$
$$= 4\times10^{-18}\ \text{m}W/Hz$$

$$PSD_{thermal}@290K = -174\ dBm/Hz$$

Cascade Analysis

$$G_N = \prod_{n=1}^{N} G_n$$

$$G_N(dB) = \sum_{n=1}^{N} G_n$$

$$NF_N = NF_1 + \sum_{n=2}^{N} \frac{NF_n - 1}{\prod_{j=1}^{n-1} G_j}$$

$$= NF_1 + \frac{NF_2 - 1}{G_1} + \frac{NF_3 - 1}{G_1 G_2} + \cdots + \frac{NF_N - 1}{G_1 G_2 \cdots G_{N-1}}$$

$$NF_N(dB) = 10\log\left\{NF_1 + \sum_{n=2}^{N} \frac{NF_n - 1}{\prod_{j=1}^{n-1} G_j}\right\}$$

$$\frac{1}{OIP3_{casc}} = \frac{1}{G_2 \bullet OIP3_1} + \frac{1}{OIP3_2}$$

$$\frac{1}{OIP3_{cacs}} = \left\{\sum_{\substack{n=1 \\ N\geq 2}}^{N-1}\left[\left(OIP3_n \prod_{k=n+1}^{N} G_k\right)\right]^{-1} + OIP3_N^{-1}\right\}$$

$$OIP3_{casc} = \frac{G_2 \bullet OIP3_1 \bullet OIP3_2}{G_2 \bullet OIP3_1 + OIP3_2}$$

$$\xrightarrow[G_2 \bullet OIP3_1 >> OIP3_2]{} OIP3_2$$

$$\xrightarrow[G_2 \bullet OIP3_1 << OIP3_2]{} G_2 \bullet OIP3_1$$

Appendix 2: RF Gain of a TIA

The RF gain of a transimpedance-amplified photoreceiver, given the transimpedance gain, is calculated as follows. If the photodetector output is connected directly to an external load *Z*, as shown in Fig. A2(a), the RF power is given by

$$P_1 = i^2 Z/2$$

where *i* is the peak RF photocurrent. With a transimpedance amplifier in place (Fig. A2(b)) having transimpedance gain *R*(V/A), the RF power at the TIA output is

$$P_2 = v^2/2Z \ .$$

But $v = Ri$, hence, the RF gain is

$$G = \frac{P_2}{P_1} = \frac{R^2 i^2/2Z}{i^2 Z/2} = \frac{R^2}{Z^2}$$

For example, *R* = 500 corresponds to *G* = 100 (20 dB) for *Z* = 50 ohms.

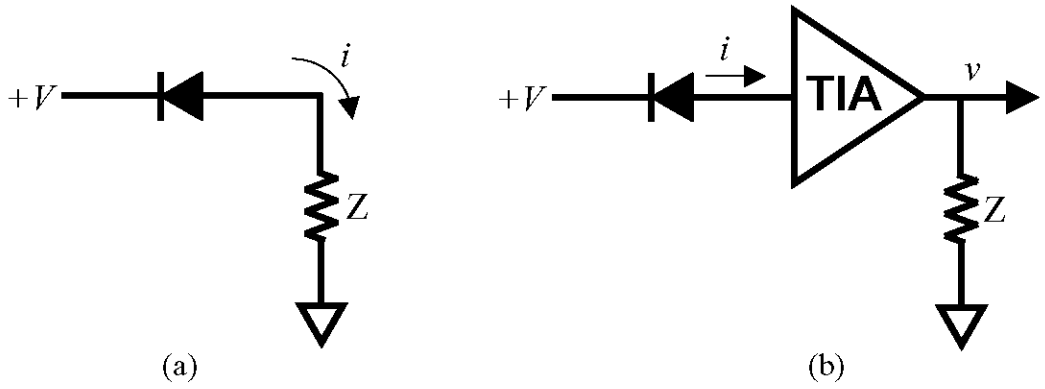

Fig. A2. Circuit model used to calculate the RF gain of a TIA.

Appendix 3: Summary of Device & System RF Parameters

(Based on manufacturer's data and in-house laboratory measurement)

A. RF Amplifier (Miteq M/N AM-4A-0510)

Gain (1 GHz)	+56 dB
NF(1 GHz)	1.6 dB
OIP3 (1 GHz)	+ 23.7 dBm

B. TIA Amplifier (Discovery DSC R402AC)

R (V/A)	601.4 ohms
Gain (1 GHz)	+21.6 dB (calculated)
NF (1 GHz)	3 dB
OIP3 (1 GHz)	+ 37 dBm (nominal)
R(A/W)	0.7

C. Bare Photonic Link ($V_\pi = 5.6V @ 1\,GHz$)

Gain (1 GHz, 0.9 mA)	–37.8 dB	
NF	+39.3 dB	(calculated)
OIP3 (1 GHz, 0.9 mA)	–16 to –14 dBm	
Gain (1 GHz, 92 uA)	–59 dB	(calculated)
NF	+39.3 dB	(calculated)
OIP3 (1 GHz, 92 uA)	–33.7 dBm	(calculated)
Gain (1 GHz, 100 uA)	–51.9 dB	(calculated, no internal Z)
OIP3 (1 GHz, 100 uA)	–27.0 dBm	(calculated, no internal Z)

D. RF - Amplified Photonic Link

Gain (1 GHz,92uA)	–2.3 dB
NF(1 GHz)	+59.7 dB
OIP3 (1 GHz)	+18 to +19 dBm

E. TIA - Amplified Photonic Link

Gain (1 GHz, 100uA)	–29.7 dB
NF(1 GHz)	+45 dB
OIP3 (1 GHz)	–6.9 to –7.8 dBm